FAST FACTORIZED BACKPROJECTION ALGORITHM FOR UWB SAR IMAGE RECONSTRUCTION

*Viet T. Vu, Thomas K. Sjögren, Mats I. Pettersson**

Blekinge Institute of Technology, Campus Gräsvik, 37179 Karlskrona, Sweden

ABSTRACT

The fast factorized backprojection for bistatic SAR algorithm (BiFFBP), which processes the bistatic SAR data in more than one beam forming stage, is presented in this paper. The algorithm is developed on the bistatic fast backprojection algorithm SAR (BiFBP) and inherits time-domain characteristics such as unlimited scene size, real time processing, local processing, manageable motion compensation, and large range migration handling. Also, the algorithm works well with different kinds of bistatic configuration. For these reason, it is very suitable for UWB bistatic SAR processing. The proposed algorithm is tested successfully with simulated UWB bistatic SAR data.

Index Terms— algorithm, bistatic, fast backprojection, fast factorized backprojection, UWB

1. INTRODUCTION

Bistatic synthetic aperture radar (SAR) systems refer to SAR systems utilizing separated transmitter and receiver(s). Bistatic SAR systems can be built from the existing monostatic SAR systems. For example, the hybrid bistatic SAR system is constructed with TerraSAR-X satellite and the airborne SAR-sensor PAMIR [1] or the airborne bistatic systems SAR system developed on LORA and SETHI [2]. In most cases, processing SAR data normally requires much effort and sometimes may only be performed at ground stations. However, this can be easily handled with the flexibility in deploying receiver(s) of bistatic SAR systems. With the multiple deployed receivers, a target or a ground scene can be observed at different angles with a bistatic SAR system. This enhances the classification ability of the target. From a system designer's point of view, the design of bistatic SAR is more flexible than of monostatic SAR and the cost to build a bistatic SAR can therefore be minimized.

With unique advantages, bistatic SAR becomes a research topic of interest. This can be shown by a large number of publications concerning this topic. Modifications of the monostatic SAR algorithms such as range doppler (RD), range migration (RM), and chirp scaling (CS) have been focused for long time. Among these algorithm, only nonlinear CS is declared to handle general cases of bistatic configuration [3]. However, frequency-domain algorithms in general and nonlinear CS in particular are not very suitable for ultrawideband ultrawidebeam (UWB) SAR systems. Herein, UWB SAR refers to SAR system utilizing large fractional signal bandwidth and wide integration angle associated with wide antenna beamwidth. The challenges in UWB SAR data processing can be found in huge amount of data, large range migration, real time processing, and big motion error. Such processing usually relies on the time-domain algorithms like global backprojection (GBP).

In [4], bistatic global backprojection (BiGBP) is shown to work perfectly with bistatic UWB SAR systems. However, the huge computational burden required by BiGBP makes this algorithm inefficient. Also in [4], the bistatic fast backprojection algorithm (BiFBP) is proposed. Similar to BiGBP, this algorithm owns time-domain characteristics such as unlimited scene size, real time processing, local processing, manageable motion compensation, large range migration handling, and is not limited by any bistatic configuration.

The objective of this paper is to present the bistatic fast factorized backprojection algorithm (BiFFBP) in an analytical way. This objective different from the [2] where the experimental results have been focused. Also, the beam center line in [2] passes through the middle of a subimage along a direction perpendicular to an ellipse while the beam center line in this paper is defined by the middle of the subimage and the center of the ellipse. Like BiFBP, BiFFBP reconstructs a SAR image on a subaperture and subimage basis. The processing of BiFFBP is therefore divided into two stages: beam forming and local backprojection. Unlike BiFBP utilizing a unique beam forming stage, there is more than one beam forming stage used in BiFFBP. This kind of processing allows us to further reduce processing time.

The paper is organized as follows. Section 2 reviews the fast time-domain BiFBP algorithm which is the basis for the development of the new algorithm BiFFBP. The BiFFBP algorithm is presented in Section 3. Simulation results and evaluations for the proposed algorithm are given in Section 4. Section 5 provides the conclusions.

*The authors would like to thank the KK-Foundation for the financial support in this research project, the Swedish Defence Research Agency, Saab Bofors Dynamics, Saab Electronic Defence Systems and RUAG Space for their cooperation.

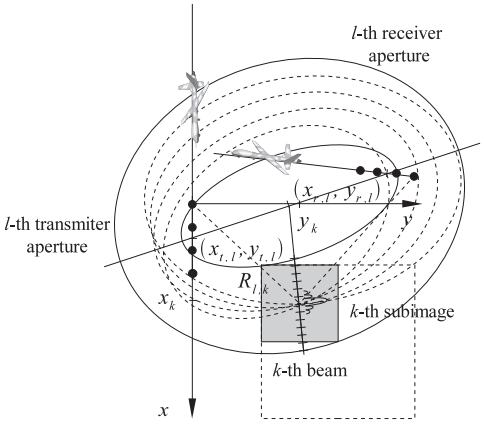

Fig. 1: The beam forming stage in BiFBP. In this illustration, the $k-$th beam covering the $k-$th subimage is formed from all radar echo in the $l-$th subapertures.

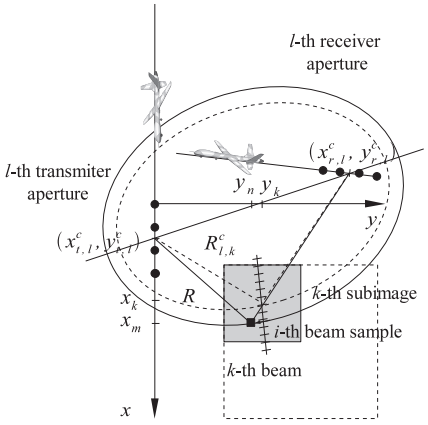

Fig. 2: The backprojection stage in BiFBP. In this illustration, the $k-$th subimage is mapped by the $k-$th beam samples of the $l-$th subapertures over an ellipsoidal mapping.

2. BISTATIC FBP

BiFBP, a fast time-domain algorithm, is recently introduced in [1]. The algorithm reconstructs a bistatic SAR image on a subaperture and subimage basis. This kind of processing reduce processing time and basically overcome the major shortcoming of BiGBP. For a reconstructed SAR scene of $N \times N$ with N aperture positions, BiFBP is stated to run approximately $\sqrt{N}$ times faster than BiGBP.

For time-domain algorithms in general and for BiFBP in particular, the illuminated scene is supposed to be reconstructed on the ground plane instead of the range plane to simplify range calculations. For local processing, the full imaged scene is segmented into K subimages while the complete transmitter and receiver apertures are split into L subapertures. The reconstruction of the imaged scene is processed in two stages: beam forming and backprojection.

In the beam forming stage, all radar echo belonging to the $l-$th transmitter and receiver subapertures are first shifted with respect to the center of the $k-$th subimage and then superposed to form the $k-$th beam. This superposition is interpreted as the projection of the data samples into the beam samples in a linear superposition as illustrated in Fig. 1. The number of beam range samples is selected to be just enough to cover the whole subimage limited by two dotted-dashed ellipses.

The $k-$th subimage is then backprojected from the $k-$th beam in the backprojection stage. The backprojection is performed over an ellipsoidal mapping. The $l-$th centers of the transmitter and receiver subapertures determine the foci of the ellipsoid. The major axis is defined by the line between the two foci. The major diameter of the ellipsoid is given by a range R as illustrated in Fig. 2. This procedure will be repeated for all subapertures. The full SAR image is finally retrieved by a coherent combination of all subimages. A mathematical expression of BiFBP is given by

$$h\left(x_m, y_n\right) = \bigcup_{k=1}^{K} \sum_{l=1}^{L} \int_{t_l - \frac{t_s}{2}}^{t_l + \frac{t_s}{2}} g\left(v_t t, v_r t, \mathrm{c}\tau - R_{l,k} + \left(R - R_{l,k}^c\right)\right) dt \tag{1}$$

where t_l is the time instant corresponding to the $l-$th centers of the subapertures and t_s the integration time along the subapertures. The speed of the transmitter and receiver platforms are indicated by v_t and v_r, respectively, c is the speed of light, and $g\left(t, \tau\right)$ denotes the range-compressed radar echoes. The major diameter of the ellipsoid which is used to backproject a beam sample to a SAR image pixel (x_m, y_n) is defined by R. The range from an aperture position of the $l-$th transmitter subaperture via the center of the $k-$th subimage to the corresponding position of the $l-$th receiver subaperture is given by $R_{l,k}$ while $R_{l,k}^c$ is the center range, i.e. refers to the center of the $l-$th transmitter and receiver subapertures.

3. BISTATIC FFBP

BiFBP described in the previous section has been shown to work with any bistatic configuration and be suitable for UWB SAR systems. The processing time of the algorithm can also be proved to be much shorter than BiGBP due to the processing on a subaperture and subimage basis. However, there exist other methods which can further reduce processing time such as factorization, i.e. processing data in multiple beam forming stages. In this section, we present the BiFFBP algorithm in an analytical way. Similar to BiFBP, the bistatic SAR data is processed on a subaperture and subimage basis. However, BiFFBP performs multiple beam forming stages before the

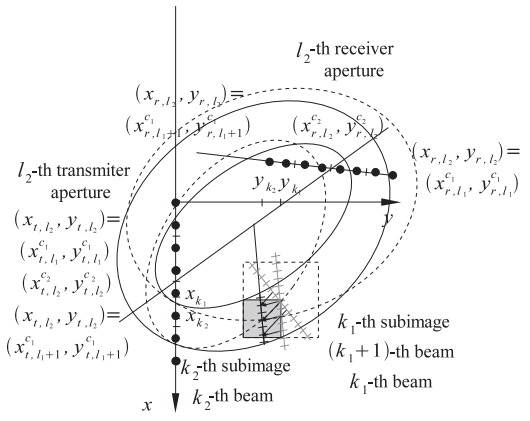

Fig. 3: The second-order beam formation in BiFFBP. The L_1/L_2 first-order beams are first shifted and then added together in a linear superposition to created a second-order beam. In this illustration, $L_1/L_2 = 2$ and $K_2/K_1 = 4$.

backprojection stage. This reduces the processing time from $\sqrt{N}$ to $\log(N)$.

In the first beam forming stage, the same procedure as for BiFBP is handled. The full imaged scene as well as the complete transmitter and receiver apertures are divided into K_1 first-order subimages and L_1 first-order subapertures. To form the k_1-th first-order beam, the bistatic SAR data belonging to the l_1-th subaperture is first shifted with respect to the center of the k_1-th subimage then superposed

$$b_1\left(t_{l_1}, \mathrm{c}\tau - R_{l_1,k_1}\right) = \int_{t_{l_1}-\frac{t_s}{2}}^{t_{l_1}+\frac{t_s}{2}} g\left(v_t t, v_r t, \mathrm{c}\tau - R_{l_1,k_1}\right) dt \tag{2}$$

where t_{l_1} is the time corresponding to the l_1-th centers of the subapertures and t_s the integration time along the subapertures. The range R_{l_1,k_1} from an aperture position of the l_1 transmitter subaperture (x_{t,l_1}, y_{t,l_1}) via the center of the k_1 subimage (x_{k_1}, y_{k_1}) to the corresponding aperture position of the l_1 receiver subaperture (x_{r,l_1}, y_{r,l_1}) is determined by

$$\begin{aligned} R_{l_1,k_1} &= \sqrt{\left(x_{t,l_1}-x_{k_1}\right)^2 + \left(y_{t,l_1}-y_{k_1}\right)^2 + h_t^2} + \\ &\quad \sqrt{\left(x_{r,l_1}-x_{k_1}\right)^2 + \left(y_{r,l_1}-y_{k_1}\right)^2 + h_r^2} \end{aligned} \tag{3}$$

After the first beam forming stage, $K_1 \times L_1$ first-order beams are generated covering K_1 subimages. The number of beam samples must be selected large enough to cover the beams created in the next beam forming stages.

In the second beam forming stage, the first-order beams are used to form second-order beams. A first-order subimage is further segmented into a number of smaller second-order subimages. The number of subimages therefore increases to K_2. Conversely, a number of first-order transmitter subapertures is combined together to form larger a second-order subaperture. This step is also applied to the same number of first-order receiver supapertures. Thus, the number of subapetures is reduced to L_2. To form the l_2-th second-order beam, L_1/L_2 first-order beams are first shifted with respect to the center of the k_2-th subimage and then superposed

$$\begin{aligned} &b_2\left(t_{l_1}, \mathrm{c}\tau - R_{l_1,k_1} - R^{c_1}_{l_1,k_2} + R^{c_1}_{l_1,k_1}\right) = \\ &\sum_{l_1=1+(l_2-1)\frac{L_1}{L_2}}^{l_2\frac{L_1}{L_2}} b_1\left(t_{l_1}, \mathrm{c}\tau - R_{l_1,k_1} - \left(R^{c_1}_{l_1,k_2} - R^{c_1}_{l_1,k_1}\right)\right) \end{aligned} \tag{4}$$

where

$$\begin{aligned} R^{c_1}_{l_1,k_1} &= \sqrt{\left(x^{c_1}_{t,l_1}-x_{k_1}\right)^2 + \left(y^{c_1}_{t,l_1}-y_{k_1}\right)^2 + h_t^2} + \\ &\quad \sqrt{\left(x^{c_1}_{r,l_1}-x_{k_1}\right)^2 + \left(y^{c_1}_{r,l_1}-y_{k_1}\right)^2 + h_r^2} \end{aligned} \tag{5}$$

and

$$\begin{aligned} R^{c_1}_{l_1,k_2} &= \sqrt{\left(x^{c_1}_{t,l_1}-x_{k_2}\right)^2 + \left(y^{c_1}_{t,l_1}-y_{k_2}\right)^2 + h_t^2} + \\ &\quad \sqrt{\left(x^{c_1}_{r,l_1}-x_{k_2}\right)^2 + \left(y^{c_1}_{r,l_1}-y_{k_2}\right)^2 + h_r^2} \end{aligned} \tag{6}$$

Fig. 3 illustrates the second beam forming stage of BiFFBP where $K_2/K_1 = 4$ and $L_1/L_2 = 2$. As shown, the k_2-th beam is formed from the first-order k_1-th and $(k_1+1)-$th beams. After the second beam forming stage, $K_2 \times L_2$ second-order beams are generated covering K_2 subimages. Similarly, in the next beam forming stages, higher order beams are formed from lower order beams. This step is repeated until the final beam forming stage.

Assuming that BiFFBP only has two beam forming stages, the second-order beams are used to backproject into the K_2 subimages. Similar to BiFBP, the backprojection is carried out over an ellipsoidal mapping. The l_2-th centers of the transmitter and receiver subapertures determine the foci of the ellipsoid and the major axis of the ellipsoid is the line going through these foci. The backprojecting the i_2-th sample of the k_2-th second-order beam to the image pixel (x_m, y_n) belonging to the k_2-th second-order beam is represented by

$$\begin{aligned} &h_{k_2}(x_m, y_n) = \\ &\sum_{l_2=1}^{L_2} b_2\left(t_{l_1}, \mathrm{c}\tau - R_{l_1,k_1} - R^{c_1}_{l_1,k_2} + R^{c_1}_{l_1,k_1} - R + R^{c_2}_{l_2,k_2}\right) \end{aligned} \tag{7}$$

where

$$\begin{aligned} R^{c_2}_{l_2,k_2} &= \sqrt{\left(x^{c_2}_{t,l_2}-x_{k_2}\right)^2 + \left(y^{c_2}_{t,l_2}-y_{k_2}\right)^2 + h_t^2} + \\ &\quad \sqrt{\left(x^{c_2}_{r,l_2}-x_{k_2}\right)^2 + \left(y^{c_2}_{r,l_2}-y_{k_2}\right)^2 + h_r^2} \end{aligned} \tag{8}$$

and

$$R = \sqrt{\left(x_{t,l_2}^{c_2} - x_m\right)^2 + \left(y_{t,l_2}^{c_2} - y_n\right)^2 + h_t^2} + \sqrt{\left(y_{r,l_2}^{c_2} - x_m\right)^2 + \left(y_{r,l_2}^{c_2} - y_n\right)^2 + h_r^2} \quad (9)$$

Over an ellipsoid mapping, the image pixels, which define the same travel distance R or are crossed by the solid ellipse with the major diameter R and belong to the k_2- th subimage, are mapped by the i_2-th sample of the k_2-th second-order beam. This procedure will be repeated for all L_2 subapertures. Finally, K_2 second-order subimages are arranged to build up K_1 first-order subimages. These K_1 first-order subimage are again coherently combined to reconstruct the full reconstructed SAR scene

$$h(x_m, y_n) = \bigcup_{k_1=1}^{K_1} \bigcup_{k_2=1+(k_1-1)\frac{K_2}{K_1}}^{k_1\frac{K_2}{K_1}} h_{k_2}(x_m, y_n) \quad (10)$$

4. SIMULATION RESULTS AND EVALUATIONS

In this section, we show some simulation results to demonstrate and evaluate BiFFBP. The parameters of CARABAS-II and LORA are used in the simulation [4]. The transmitter is assumed to be carried by CARABAS-II and the receiver by LORA. An angle of 60^o formed by two flight tracks is selected. The considered aperture includes 4096 aperture positions ($N_l = 4096$). The ground scene is simulated by a number of point-like scatters equally spaced. The reconstructed SAR scene is limited by 1024 m$\times$1024 m. If the image pixel is chosen by 1 m$\times$1 m, the number of image samples is given by $N_k^2 = 1024^2$.

Fig. 4.a shows the SAR scene which is reconstructed with BiFBP. $L = 64$ and $K = 256$ are selected for BiFBP. In this SAR image, the scatters are well focused and appear as the point targets. Their general features, i.e. point-like scattering, orthogonal and non-orthogonal sidelobes, are very similar to monostatic SAR. However, the point targets are inclined with an angle. This inclination is supposed to be dependent of the motion parameters of the transmitter and receiver platforms.

The SAR scene is again reconstructed with the proposed algorithm BiFFBP and shown Fig. 4.b. In this demonstration, BiFFBP has two beam forming stage. The same parameters as BiFBP are selected for the first beam forming stage of BiFFBP, i.e. $L_1 = 64$ and $K_1 = 256$. In the second beam forming stage, we segment one first-order subimage into four second-order subimages, i.e. $K_2/K_1 = 4$, and combine two first-order subapertures into one second-order subaperture, i.e. $L_1/L_2 = 2$. Thus, $K_2 = 1024$ and $L_2 = 32$. As observed, all scatters are still well focused in the SAR image. There is no clear difference between the SAR images reconstructed with BiFBP and BiFFBP. This result also indicates that BiFFBP is valid for UWB bistatic SAR systems.

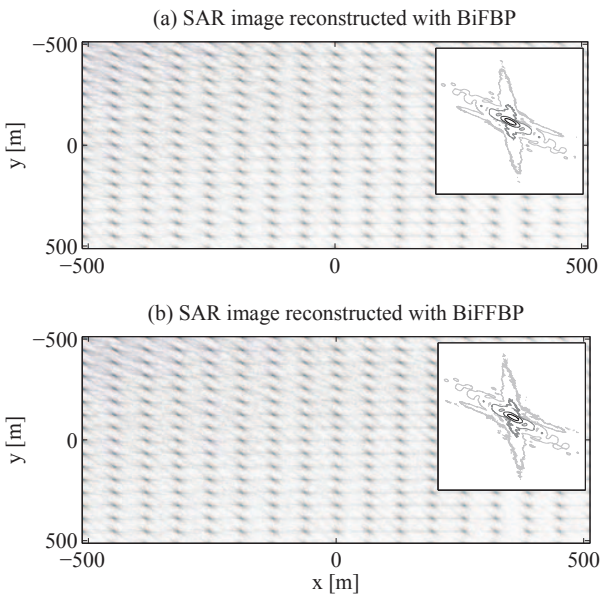

Fig. 4: The UWB bistatic SAR images of the ground scene reconstructed with the algorithms. (a) BiFBP, (b) BiFFBP.

5. CONCLUSION

In this paper, we present a new algorithm BiFFBP to process UWB bistatic SAR. BiFFBP works in time-domain and therefore inherit the time-domain characteristics and is not limited by any bistatic SAR configuration. BiFFBP processes bistatic SAR data in a subaperture and subimage basis. In addition, the factorization method is applied in BiFFBP. The proposed algorithm is tested with simulated UWB bi-static SAR data based on the CARABAS-II and LORA parameters.

6. REFERENCES

[1] I. Walterscheid, J. H. G. Ender, J. Klare, A. R. Brenner, O. Loffeld, "Bistatic image processing for a hybrid SAR experiment between TerraSAR-X and PAMIR," in *Proc. IEEE IGARSS*, 2006, pp. 1934–1937.

[2] L. M. H. Ulander, P.-O. Frölind, A. Gustavsson, D. Murdin, and G. Stenström, "Fast factorized back-projection for bistatic SAR processing," in *Proc. EUSAR*, 2010, pp. 4(p).

[3] F.H. Wong, I.G. Cumming, and Yew Lam Neo, "Focusing bistatic SAR data using the nonlinear chirp scaling algorithm," IEEE Trans. Geosci. Remote Sensing, vol. 46, no. 9, pp. 2493–2505, September 2008.

[4] V. T. Vu, T. K. Sjögren, and M. I. Pettersson, "Fast back-projection for UWB bistatic SAR," in *Proc. IEEE Radarcon*, 2011, pp. (4p), accepted for publication.